Synthesis of Ti(C, N, O) from TiO2 by CH4-H2-N2 Gas Mixture at Low Temperature

Gangqiang Fan
Chongqing University
Youling Hou
Chongqing University
Dejun Huang
Malvern Panalytical Ltd
Jie Dang (jiedang@cqu.edu.cn)
Chongqing University
Run Zhang
Chongqing University
Junyi Xiang
Chongqing University
Xuewei Lv
Chongqing University
Xiaoming Ding
National Innovation (Qingdao) High speed Train Material Institute Co. LTD

Research Article

Keywords: Ti(C, N, O), TiO2, CH4-H2-N2 gas mixture, novel synthesis process

Posted Date: May 17th, 2021

DOI: https://doi.org/10.21203/rs.3.rs-520202/v1

Synthesis of Ti(C, N, O) from TiO_2 by CH_4-H_2-N_2 Gas Mixture at Low Temperature

Gangqiang Fan[1,3], Youling Hou[1,3], Dejun Huang[4], Jie Dang[1,2,*], Run Zhang[1,3], Junyi Xiang[1,*], Xuewei Lv[1,3], Xiaoming Ding[5]

1 College of Materials Science and Engineering, Chongqing University, Chongqing 400044, PR China

2 State Key Laboratory of Advanced Processing and Recycling of Non-ferrous Metals, Lanzhou University of Technology, Lanzhou, 730050, PR China

3 Chongqing Key Laboratory of Vanadium-Titanium Metallurgy and New Materials, Chongqing University, Chongqing 400044, PR China

4 Spectris Instr. & Sys. Shanghai Ltd., Malvern Panalytical (China), Shanghai 200233, PR China

5 National Innovation (Qingdao) High speed Train Material Research Institute Co. LTD, Qingdao266109, China

***Corresponding author**: Jie Dang, Junyi Xiang

E-mail: jiedang@cqu.edu.cn, xiangjunyi@cqu.edu.cn

Phone: +86-23-65112631; Fax: +86-23-65112631

Address: College of Materials Science and Engineering, Chongqing University, Chongqing 400044, PR China

ORCID iD: https://orcid.org/0000-0003-1383-8390

Abstract

Titanium carbides, oxides, nitrides and carbonitrides possess many special and excellent properties. But the high production cost caused by the traditional carbothermic reduction process severely limits the wide applications. In this study, a novel synthesis process has been proposed by reducing and carbonitriding TiO_2 with CH_4-H_2-N_2 gas mixture at low temperatures. The synthesis of Ti(C, N, O), reaction mechanism and the products composition have been investigated. Thermodynamic analysis indicated that TiO_2 could be ultimately reduced and carbonitrided to Ti(C, N, O) by CH_4-H_2-N_2 gas mixture. Based on the predictions of thermodynamics, the effects of reduction time, temperature, and gas composition have been studied experimentally. The obtained results indicated that increasing reduction temperature and introduction of N_2 are beneficial to the synthesis of Ti(C, N, O). Finally, the optimum reaction conditions have been obtained. The density functional theory (DFT) results further demonstrated the reaction mechanism. This work provides a new approach to prepare metallic carbonitrides from their oxides.

Keywords: Ti(C, N, O); TiO_2; CH_4-H_2-N_2 gas mixture; novel synthesis process

1. Introduction

Titanium carbides, nitrides, oxides, and their solid solutions (TiC, TiN, Ti(C, N, O)) are the leading advanced engineering ceramics that can be used in metal-working, electrical and electronic, automotive, chemical, and refractory industries [1-5], due to their special properties such as low density, high melting points, and hardness, high-temperature strength retention, good conductivity, excellent oxidation and wear resistance, and low thermal expansion coefficient in coating and thin films [6]. Titanium carbide can also be used as catalytical and electrochemical material [7]. A potential application is that titanium carbide, oxide, nitride, and their solid solution can be used as the raw material (soluble anode) for producing metallic titanium [8-11].

Industrially, TiC is usually synthesized from TiO_2 by carbothermic reduction process; while the synthesis of TiN is based on the reaction of Ti or TiH_2 powders with N_2 or NH_3, at 1000 ºC to 1400 ºC; Ti(C, N) is usually made of the diffusion of TiC with TiN powders at 1700 ºC to 1800 ºC. The reaction process can be described as the following reactions:

$$TiO_2\ (s) + 3C\ (s) = TiC\ (s) + 2CO\ (g) \quad (1)$$

$$Ti\ (s) + 0.5N_2\ (g) = TiN\ (s) \quad (2)$$
$$TiH_2\ (s) + N_2\ (g) = TiN\ (s) + H_2\ (g) \quad (3)$$
$$Ti\ (s) + NH_3\ (g) = TiN\ (s) + 1.5H_2\ (g) \quad (4)$$
$$TiH_2\ (s) + NH_3\ (g) = TiN\ (s) + 2.5H_2\ (g) \quad (5)$$
$$TiC\ (s) + TiN\ (s) = Ti(C, N)\ (s) \quad (6)$$

Under the standard condition, reaction (1) occurs at a temperature of 1564 K (1291 ^{o}C). Besides, reaction (1) requires a large supply of heat to complete this reaction because of the strongly endothermic nature of the reaction ($\Delta H_{(1)}$ = 518.5 kJ/mol, T = 1291 ^{o}C). In industrial production, the reaction usually occurs at 1700 ^{o}C to 2100 ^{o}C for 10 to 24 hours, or even longer time. Even though $\Delta G_{(2)\sim(5)} < 0$, the high cost of raw materials (Ti powder and TiH_2 powder) leads to the high cost of products. To obtain a high-quality product, the process usually needs to continue for more than 30 hours. The synthesis of Ti(C, N) is limited by the quality of TiC and TiN as well.

To address these issues, many researchers have put forward a lot of methods, such as the gas-solid reaction of $TiCl_4$ with CaC_2 [12], the gas-liquid reaction of $TiCl_4$ with $NaNH_2$ [13], the gas-gas reaction of $TiCl_4$ with CH_4 (N_2) gas [14, 15], the sol-gel process of $TiCl_3$ with polyacrylonitrile and dimethylformamide [16], and other methods [17]. But none of them has been used for commercial production so far, due to the high cost and low quality of $TiCl_4$ and $TiCl_3$ as raw material, which need to go through a complex treatment process from TiO_2 or titanium bearing mineral. Oyama et al [18] reported that the transition-metal oxides could be reduced into their carbides and nitrides by methane, hydrogen, and ammonia gas. Zhang and Ostrovski [19] also showed that TiC could be prepared from TiO_2 and ilmenite with CH_4-bearing gas mixture. Our previous researches [20-25] also exhibit the tremendous advantage of this method for titanium oxycarbide and titanium oxycarbonitride production compared with the traditional process. However, the reduction mechanism and the product composition have not been clarified clearly, and are needed to further study.

Therefore, based on our previous work, the effects of N_2 addition and reaction temperature on the reduction of TiO_2 with CH_4-containing gas mixture, and the reduction products composition under different conditions have been studied in the present work. The thermodynamic and first-principles calculations have also been carried out to achieve a deep understanding of the reduction process.

2. Experimental

2.1 Materials

TiO_2 and Fe_2O_3 powders are both the analytical reagent (AR) with 99% purity (Chengdu Kelong Corporation, China). The CH_4, H_2, N_2, and Ar gases used in this study as the reaction gas and protective gas are with 99.999% purity (Chongqing Ruike Corporation, China).

2.2 Experimental

The raw materials were mixed in a certain proportion after dried at 200 °C for more than 24 hours to remove the water in the raw materials. Around 0.5 g powders were loaded in a corundum crucible with a 30 mm diameter and 5 mm height, placed inside the vertical tube furnace. The furnace was then heated up to the desired temperature at a 5 °C/min rate. CH_4, N_2, and H_2 gas mixtures were introduced into the furnace from the top at the desired temperature, while Ar gas was blown into the furnace during the heating and cooling procedures. The flow rate of gas was precisely controlled by gas flow controllers (Alicat, Model MC-500SCCM-D, and MC-1SLPM-D). The device and the schematic diagram have been described elsewhere [22].

2.3 Analytical methods

After the carbonitriding procedure, the product would be ground and mounted for the following detection. The microscopic observation was carried out by scanning electron microscope (SEM) (Quattro S, Thermo Fisher Scientific), with 20 kV accelerating voltage. The phase identification was carried out by X-ray diffraction (XRD) (PANalytical, AERIS) detection, with Cu Kα radiation. The accelerating voltage and the tube current were 40 kV and 7.5 mA respectively, and the 2θ arranged among 10 ~ 90° with an angular step of 0.0108° and 300 s of permanence. The phase analysis and the Rietveld refinement were performed in HighScore Plus 4.9 software with the ICSD database. The pseudo-Voigt function was sued in the Rietveld refinement to describe the Bragg reflection profile, and the Spherical Harmonics function was used to determine the preferred orientation of the crystal.

To investigate the competition behavior of different gas molecules on the TiO_2 surface, the Density Functional Theory (DFT) was used in this work, performed by the plane-wave pseudopotential method using the Vienna ab-initio simulation package (VASP). The generalized gradient with the Perdew-Burke-Ernzerhof function (GGA-PBE) was used to describe the exchange-correlation interaction. To obtain the accurate results, a high energy cutoff of 550 eV was set up, with a tiny force convergence of 0.02 eV/Å. The rutile TiO_2 (110) surface was modeled as a periodic slab with 5 layers, constructed in 4 × 2 supercell (p(4 × 2)) including 48 atoms, and a vacuum layer of 15

Å was added to the surface. The Brillouin zone was sampled with a 5 × 2 × 1 Monkhorst-Pack k-point grid for surface simulation. The strong onsite Coulomb repulsion among the Ti-3d electrons was described with the DFT+U scheme formulated by Dudarev et al [26], and U_{eff} was set to 4.2 eV [27]. All DFT calculations were augmented by including long-range dispersion interactions (DFT+D3) with Becke-Johnson damping [28].

The adsorption energy (ΔE_{ads}) is computed for adsorbate on the clean surface as follows: $\Delta E_{ads} = E_{adsorbat/surface} - (E_{adsorbat} + E_{surface})$, where $E_{adsorbat/surface}$ is the energy of adsorbate on the TiO_2 (110) surface, $E_{adsorbat}$ and $E_{surface}$ are energies of an isolated molecule of adsorbate and a clean TiO_2 (110) surface, respectively.

3. Thermodynamic calculation

Thermodynamic calculations for the equilibrium phases of TiO_2 in CH_4-H_2-N_2 gas mixture were performed by using FactSage software based on Gibbs free energy minimization and the database of CaO et al. [29] The equilibrium phase diagrams were calculated in the temperature range from 900 ºC to 1400 ºC in different CH_4-N_2-H_2 systems, and the equilibrium results of solid-phase were shown in **Figure 1 (a) ~ (b)** and **Figure S1** (in Electronic Supplementary Information [ESI]). **Figure 1 (a) ~ (b)** shows the phase diagram as a function of temperature with gas/TiO_2 ratio in 8 *vol*.% CH_4 – 16 *vol*.% N_2 – 76 *vol*.% H_2 system. It can be found that the final equilibrium phases depend on both the reaction temperature and gas/TiO_2 ratio. With the gas/TiO_2 ratio of 50, when T is lower than 981 ºC, C, TiN, and Ti_4O_7 exist; in the range of 981 ºC ~ 1329 ºC, TiN and C exist; in the range of 1329 ºC ~ 1344 ºC, C, Ti(C, O) and TiN exist; above 1344 ºC, Ti(C, O) and C exist. The final solid phases would also vary with the gas/TiO_2 ratio, for example, at T = 1150 ºC, the dependence of the final solid phases with the gas/TiO_2 ratio can be summarized as follows: in the gas/TiO_2 ratio range of 4.2-25, Ti(C, O) + TiN + Ti_3O_5 form; in the range of 25 ~ 26, only TiN is stable; while in the range of 26 ~ 50, the final products are Ti(C, O) + C.

Combining with equilibrium phase diagrams in different systems (described in **ESI**), it can be clearly found that the reduction of titania performs as the step by step with the gas/TiO_2 ratio increasing. In summary, the reduction sequence could be inferred as the following:

(a) in CH_4-H_2 system: TiO_2 → Magnéli → Ti_3O_5 → Ti(C,O)

(b) in CH_4-N_2-H_2 system:

At low temperature: TiO_2 → Magnéli → TiN

At middle temperature: TiO_2 → Magnéli → Ti_3O_5 → TiN/Ti(C, O) → TiN

At high temperature: TiO_2 → Magnéli → Ti_3O_5 → TiN/Ti(C, O) →Ti(C, O)

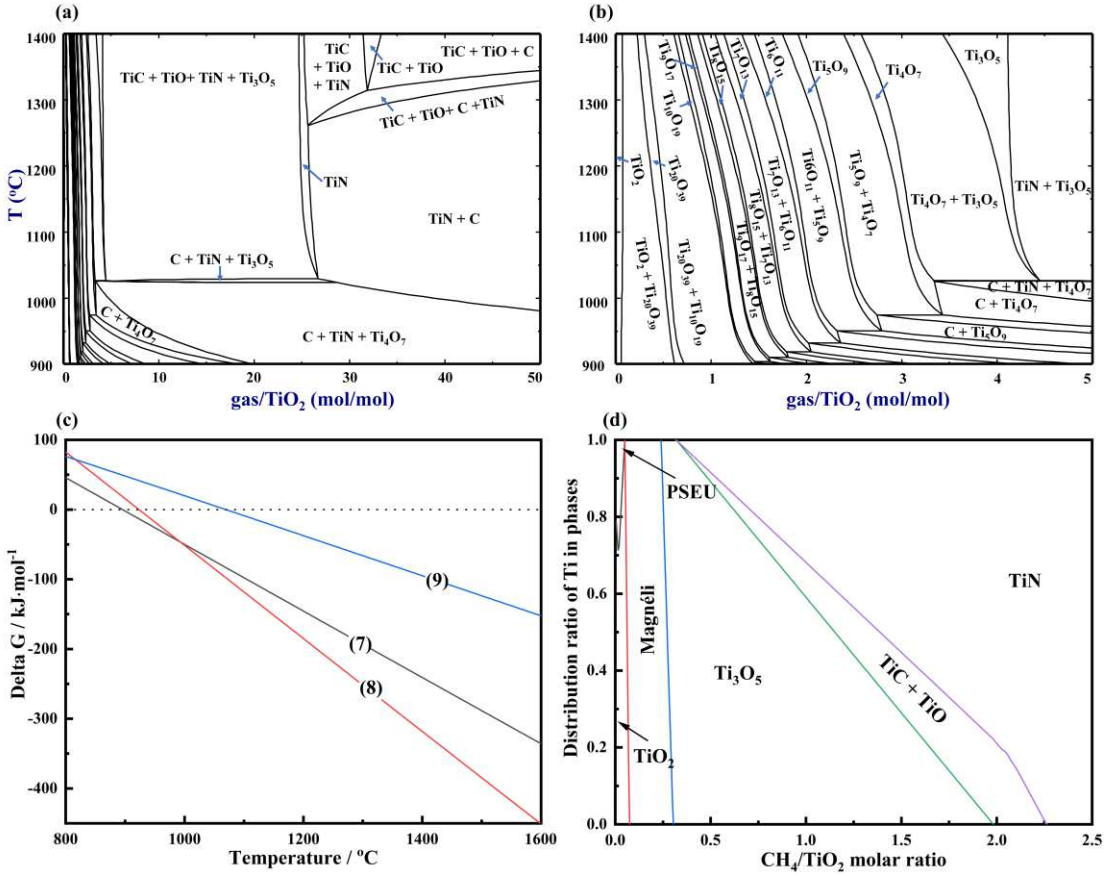

Figure 1 (a) Calculated equilibrium phase diagram of solid phases as functions of temperature and the gas/TiO_2 ratio (gas = 8 *vol*.% CH_4 – 16 *vol*.% N_2 – 76 *vol*.% H_2) and (b) partial diagram of (a); (c) the Gibbs free energy of equation (7)~ (9) as a function of temperature; (d) calculated equilibrium of titanium-bearing phases for the reaction of TiO_2 with Fe_2O_3 additive in 8 *vol*.% CH_4-8 *vol*.% N_2-84 *vol*.% H_2 gas mixture at 1200 °C.

It illustrates that at high temperature TiC or Ti(C, O) is more stable than TiN. It can be explained by the reaction Gibbs free energy of TiO_2 with CH_4-N_2-H_2 gas mixture. The possible reactions of TiO_2 with gas mixture could be expressed as follows:

$$TiO_2 + 2CH_4 + 0.5N_2 = TiN + 4H_2 + 2CO \quad (7)$$

$$TiO_2 + 3CH_4 = TiC + 6H_2 + 2CO \quad (8)$$

$$TiO_2 + CH_4 = TiO + 2H_2 + CO \quad (9)$$

The reaction standard Gibbs free energies of equation (7) ~ (9) as a function of temperature is shown in **Figure 1 (c)**. When the temperature ranges from 900 °C to 995

ºC, the standard Gibbs free energies of equation (7) is negative and less than that of equation (8); when the temperature is higher than 995 ºC, the standard Gibbs free energies of equation (8) is lower. The function of standard Gibbs free energies *vs* temperature can also indicate that the lower temperature is beneficial to the formation of TiN and the higher temperature is beneficial to the formation of Ti(C, O), consistent with the above equilibrium calculation. However, the standard Gibbs free energy of equation (9) is always higher than those of equations (7) and (8).

The effect of Fe_2O_3 additive on the reduction sequence and the phase transformation has been studied by equilibrium calculation as well. **Figure 1 (d)** shows the equilibrium results of TiO_2 with a 10 *wt.*% Fe_2O_3 additive in 8 *vol*.% CH_4-16 *vol*.% N_2-76 *vol*.% H_2 gas mixture at 1200 ºC. Combined with **Figure S2,** it can be found that there exist the titanium-ferric oxide phases (ilmenite and pseudobrookite) in the preliminary stage. At low temperatures, the titanium-ferric oxide phase exists as ilmenite ($FeTiO_3$). While at high temperatures, it exists as pseudobrookite ($FeTi_2O_5$). In $FeTiO_3$ and $FeTi_2O_5$, the valence of iron is +2, which is reduced from Fe_2O_3 by the first step calculation with CH_4 bearing gas mixture. In the first step calculation, the amount of CH_4 is 0.005 mol, with 0.01 mol N_2 and 0.0475 mol H_2, which would reduce the ferric oxide (Fe_2O_3) to ferrous oxide (FeO). The ferrous oxide would react with TiO_2 to form $FeTiO_3$ and $FeTi_2O_5$. The difference of phases existing at different temperatures may be caused by thermodynamic stability. After the ferrous oxide phase being completely reduced, the subsequent reaction is the reduction of TiO_2.

4. Results and discussions

4.1 Reaction sequence

To study the phase transformation during the reduction process, samples were reduced for different times at 1200 ºC with the total gas flow rate of 500 mL/min (8 *vol*.% CH_4 - 16 *vol*.% N_2 - 76 *vol*.% H_2). The XRD patterns of reduced samples were shown in **Figure 2 (a)**, and the detected phases were summarized in **Table S1**. During the first 10 minutes of the reduction, Ti_3O_5 as the major low-valent-titanium-bearing phase existed in the sample with residual TiO_2 and metallic iron reduced from Fe_2O_3. However, no Magnéli phase was detected in the sample. The reduction of TiO_2 to Ti_3O_5 can be divided into the reduction of TiO_2 to Magnéli phase and the reduction of Magnéli to Ti_3O_5, and it can be inferred that the reduction rate of Magnéli phase to Ti_3O_5 was faster than that of TiO_2 to Magnéli phase. It should be noted that the phase of Ti(C, N,

O) was the solid solution of TiC, TiN and TiO, due to the same crystal form [6]. In the sample reduced for 20 minutes, Ti(C, N, O) has become the major phase with rutile becoming the minor phase. With the reduction increasing to 30 minutes, Ti(C, N, O) has been detected as the only titanium-bearing major phase, with TiO_2 and Ti_3O_5 as trace phases, indicating that almost all of TiO_2 has been reduced and carbonitrided into Ti(C, N, O). Ti_3O_5 was not detected after a 1-hour reduction while TiO_2 was also detected as the trace phase in the samples reduced for 1 hour and more time. In the thermodynamic calculations and our previous research, no TiO_2 existed in the sample when Ti(C, O) formed. However, the results in this work are slightly different. It may be caused by the poor gas permeability in the crucible and internal particles. Neither $FeTiO_3$ nor $FeTi_2O_5$, which existed in the earlier reduction stage in thermodynamic calculations, was detected in samples. It may be related to the fast reduction rate of iron-containing oxides. Based on the experimental and thermodynamic results, the reduction sequence can be inferred as the following: TiO_2 → Magnéli → Ti_3O_5 → Ti(C, N, O).

The Rietveld refinement of samples reduced at 1200 °C for different times in 8 *vol*.% CH_4 - 16 *vol*.% N_2 - 76 *vol*.% H_2 were plotted as shown in **Figure 2 (b)** and **Figure S3**. As can be observed, the observed diffractogram and calculated diffractogram are in good agreement for all samples. The Bragg positions of Ti(C, N, O) were signed with magenta color. It can be seen that the Ti(C, N, O) was composed of three different solid solution phases including $TiC_{0.3}N_{0.3}O_{0.4}$ (ICSD card number #04-006-0747), $TiC_{0.4}O_{0.6}$ (ICSD card number #04-021-7421), and $TiN_{0.69}O_{0.27}$ (ICSD card number #04-006-1727) with a certain amount of vacancy as well. Because the three solid solution phases have a similar diffractogram, the diffraction peaks were signed as Ti(C, N, O). The refinement process was inspected by two targets, R_{wp} and GOF (goodness of fit), both shown in the corresponding diffractogram. The content of each titanium-bearing phase could be obtained from the refinement results as shown in **Table 1**, and the reduction degree and conversion degree of Ti (from TiO_2 to Ti(C, N, O)) could be calculated, as described by equations (10) and (11):

Reduction degree:

$$R = \frac{n_{loss-O}}{n_{Total-O}} * 100\%$$

$$= \frac{2n_{Ti} - 2n_{TiO_2} - \sum_{i=2}^{10}(2i-1)\cdot n_{Ti_iO_{2i-1}} - z\cdot n_{TiC_xN_yO_z}}{2n_{Ti}} * 100\% \quad (10)$$

$$\text{Conversion degree: } C = \frac{n_{Ti(C,\,N,\,O)}}{n_{Total-Ti}} * 100\% = \frac{n_{Ti(C,\,N,\,O)}}{n_{Ti}} * 100\% \quad (11)$$

Where n_{Ti}, n_{TiO_2}, $n_{Ti_iO_{2i-1}}$ and $n_{TiC_xN_yO_z}$ are the number moles of total Ti atom, residual TiO_2, titanium suboxide and Ti(C, N, O), respectively

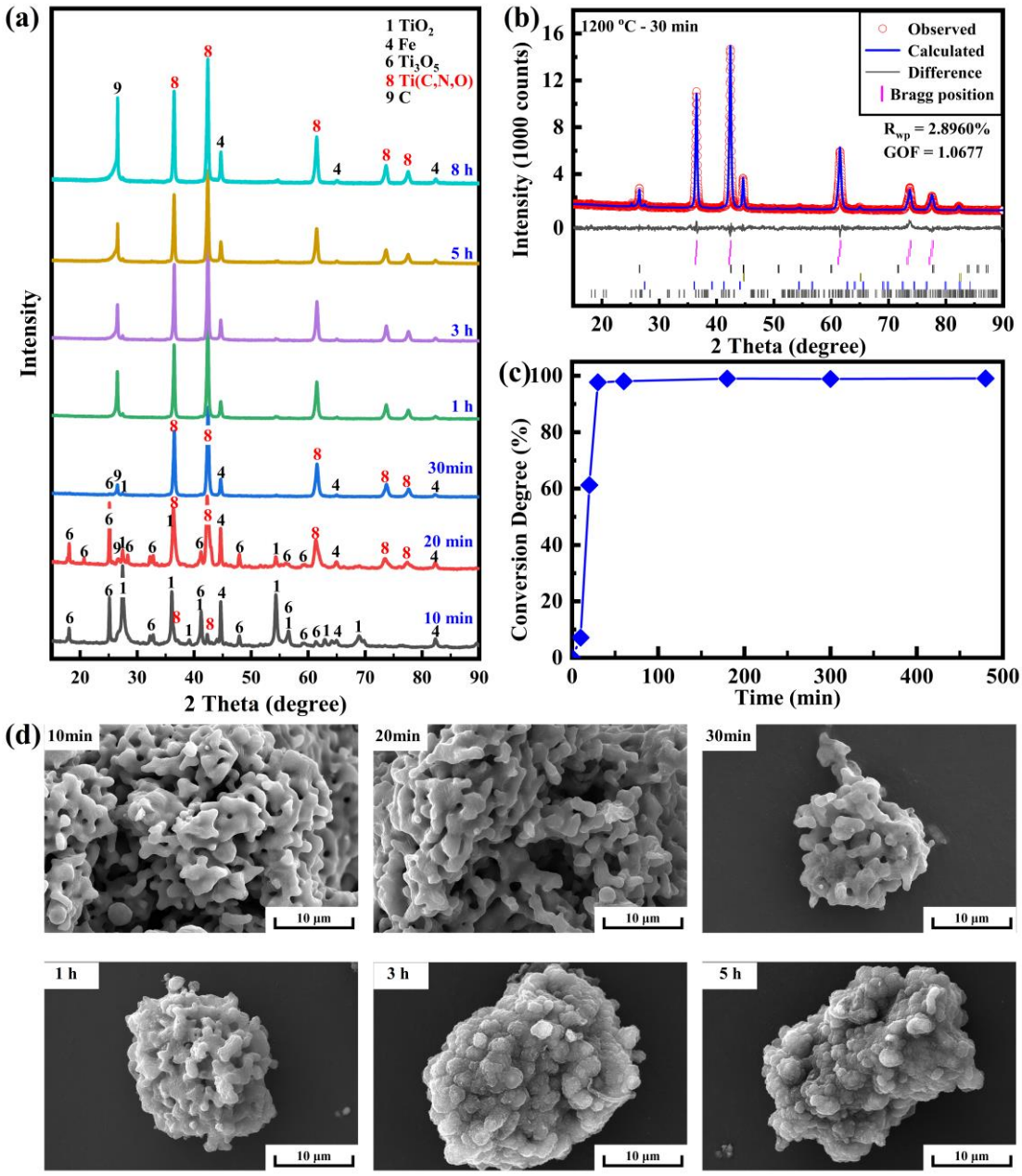

Figure 2 (a) XRD patterns of reduced samples for different reaction times at 1200 °C in 8 *vol*.% CH_4 - 16 *vol*.% N_2 - 76 *vol*.% H_2; (b) Rietveld refinement results from the XRD patterns; (c) the function of Ti conversion degree with reduction time; (d) SEM images of samples reduced for

different times.

Table 1 Quantitative results of phases bearing titanium from the Rietveld refinement (corresponding to **Figure 2** and **Figure S3**) (*wt.*%)

Time	TiO_2	Ti_3O_5	Ti(C, N, O)	Reduction degree (%)
10min	60.76	33.49	5.75	11.34
20min	11.52	31.82	56.55	51.88
30min	1.75	1.05	97.08	73.11
1h	1.50	0.88	97.87	78.78
3h	1.24	-	98.76	80.22
5h	1.39	-	98.61	84.78
8h	1.22	-	98.78	88.21

The conversion of Ti in the reduction process has also been listed in **Table S1** and shown in **Figure 2 (c)**. It is worth mentioning that the conversion of Ti represents the conversion of TiO_2 to Ti(C, N, O), not the deoxygenation extent due to the existence of oxygen in Ti(C, N, O). In the first 10 min, the conversion of Ti was just 7.14%. With the reduction time increasing to 20 min, the conversion of Ti reached 61.24%. When after 30 min, the conversion of Ti achieved 97.71%. With the reduction time extending continuously, the conversion of Ti increased slightly (60 min: 98.09 %).

The reduction degree has also been listed in **Table 1**. It can be clearly seen that the reduction degree increased drastically with the reaction time extending in the first 1 hour; however, after 1 hour, the increase rate of reduction degree lowered. The different rates indicate the different reduction stages: in the first 1 hour, it mainly contains the reduction of TiO_2 into Ti(C, N, O); after 1 hour, the deeply deoxidization of Ti(C, N, O) occurs.

The particle morphology images of samples reduced at 1200 ^oC for different times were shown in **Figure 2 (d)**. It can be seen that different morphologies were presented after different reduction times. Evidently, it presented as coralline with a porous structure for the product obtained for 10 min and 20 min, in which Ti_3O_5 is the main phase. With the reduction time extending, the particles size increased. When the reduction time was increased to 3 h, the particles aggregated and presented as spherical, and a similar morphology was observed in the sample reduced for 5 h. The deposited carbon from CH_4 attached on the surface of particles, and impeded the gas transmission into the inside of particle, so a small amount of TiO_2 is still remained.

4.2 Effect of Temperature

In our previous researches [22, 24, 25], the effect of reduction temperature on the product and reduction process has been studied, finding that higher temperature was helpful to the reduction reaction under certain conditions, but the deposited carbon cracked from methane and the sintering of particles could hinder the gas diffusion and slow down the reduction rate as well. The thermodynamic calculation also indicates that the reaction temperature has a serious impact on the reduction sequence and final product. In **Section 4.1**, almost all TiO_2 could be reduced into Ti(C, N, O) in 1 hour. Therefore, the reaction time in the experiments of the temperature effect was set as 1 hour. The inlet gas mixture was consistent with the previous experiments (8 *vol*.% CH_4 – 16 *vol*.% N_2 – 76 *vol*.% H_2). The experiments were carried out at a set of the temperature of 900 ºC, 950 ºC, 1000 ºC, 1050 ºC, 1100 ºC, 1150 ºC, and 1200 ºC, respectively. The XRD patterns of reduced samples were shown in **Figure 3 (a)** and the phases were summarized in **Table S2**.

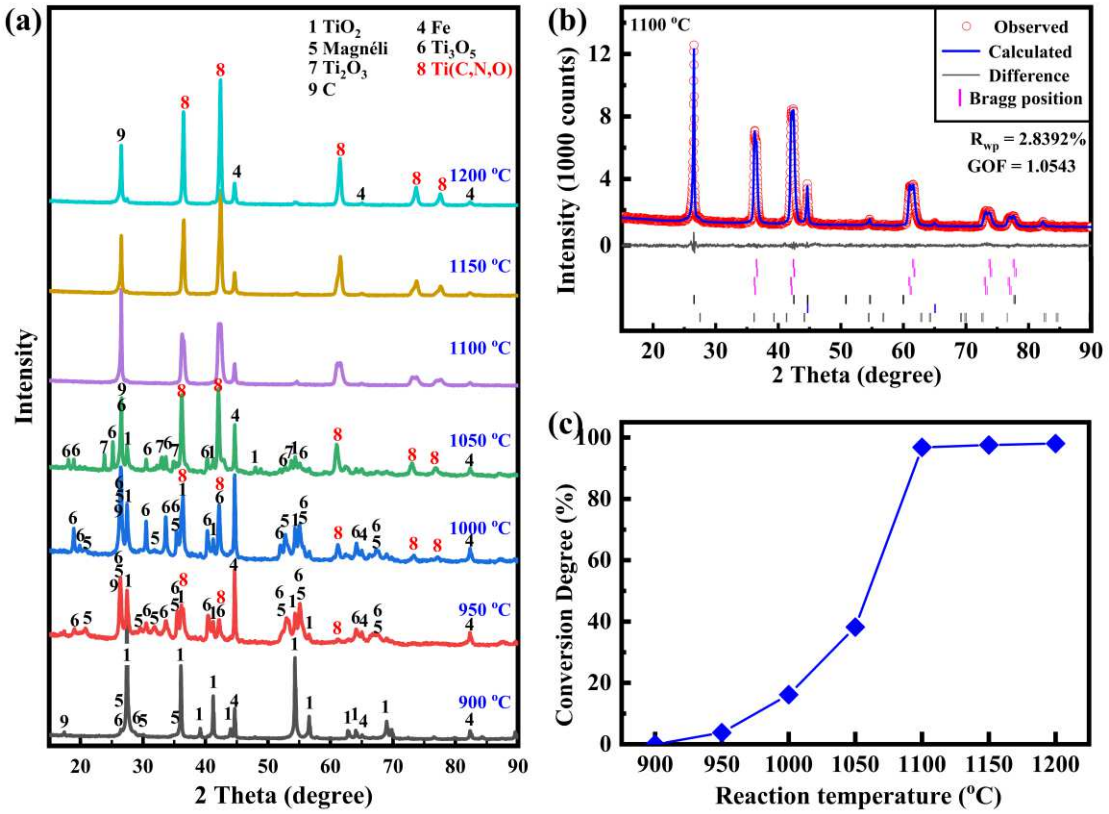

Figure 3 (a) XRD patterns of samples reduced at different temperatures for 1 h in 8 *vol*.% CH_4 - 16 *vol*.% N_2 - 76 *vol*.% H_2; (b) Rietveld refinement results from the XRD patterns; (c) the function of Ti conversion degree with the reaction temperature.

In the sample reduced at 900 ºC, the major phases were detected as TiO_2 (rutile) and Fe. With the temperature increasing to 950 ºC, Magnéli and Ti_3O_5 have become the major phases, with Ti(C, N, O) detected as a minor phase, indicating that Ti(C, N, O) started to form under this condition. Ti(C, N, O) became the major phase when reaction temperature increasing to 1000 ºC. In the sample reduced at 1050 ºC, the detected major phases contained Ti(C, N, O), Ti_3O_5, and Fe, and rutile became the minor phase. Ti_2O_3, an exceptional phase inexistence in the thermodynamic calculation at this temperature, has been detected as a minor phase. When reaction temperature increased to 1100 ºC and above, the major phases just contained Ti(C, N, O), Fe, and deposited carbon. It is worth noting that the diffraction peak of Ti(C, N, O) in the sample reduced at 1100 ºC seemingly contained two peaks, leading to the widening of the diffraction peak. In samples reduced at 1150 and 1200 ºC, the position of diffraction peak of Ti(C, N, O) was no significant change. The change of diffraction peak indicated that Ti(C, N, O) in samples treated at different temperatures was made up of different components.

Table 2 Quantitative results of phases bearing titanium from the Rietveld refinement (corresponding to **Figure 3** and **Figure S4**) (*wt.*%)

Temperature (ºC)	TiO_2	Magnéli	Ti_3O_5	Ti_2O_3	Ti(C, N, O)	Reduction degree (%)
900	73.96	10.32	15.72	-	-	3.52
950	19.18	50.11	27.60	-	3.10	13.76
1000	16.90	24.06	41.43	3.64	13.62	23.64
1050	14.59	-	33.33	9.06	43.02	54.83
1100	3.44	-	0.55	-	95.87	74.16
1150	3.05	-	-	-	96.85	77.20
1200	1.22	-			98.78	88.21

Figure 3 (b) and **Figure S4** showed the Rietveld refinements of the experimental XRD patterns of samples reduced at different temperatures for 1 h, and the quantitation of titanium-bearing phases were listed in **Table 2**. The conversion of Ti has been determined from the results, and the function of Ti conversion fraction with reduction temperature has been summarized in **Table S2** and also drawn as **Figure 3 (c)**. It is evident that the conversion degree of Ti increased with increasing the reduction temperature. Ti(C, N, O) phase can not be detected at 900 ºC but can be detected as the trace phase at 950 ºC. It indicates that the lowest temperature for forming Ti(C, N, O) is 950 ºC. With the reduction temperature increasing, the conversion degree of Ti

increases observably. At 1100 ºC, the conversion degree reaches 96.84%, and it further increases to 98.09% with temperature rising to 1200 ºC. It indicates that the optimum reduction temperature is 1100 ºC under this condition.

The reduction degree has been listed in **Table 2**. It can be seen that the reduction degree sharply increases with the reaction temperature increasing from 900 to 1100 ºC. While from 1100 ~ 1200 ºC, the reduction degree slightly increases with the increase of temperature.

4.3 Effect of N_2 addition

As discussed by thermodynamic calculation, the content of N_2 in the gas mixture has an important influence on the reduction. In the above research, all experiments were performed under the N_2 addition conditions. To further study the effect of N_2, the experiments without N_2 addition has also been investigated as a comparison, and the XRD results of TiO_2 with 10 wt.% Fe_2O_3 reduced at 1000 ºC, 1050 ºC, 1100 ºC, 1150 ºC, and 1200 ºC were shown in **Figure 4 (a)**. The Rietveld refinement results and the conversion degree of Ti has also been shown in **Figure 4 (b) ~ (c)** and **Figure S5**. In the gas mixture, the contents of CH_4 and H_2 were kept at 8 *vol.*% and 92 *vol.*% respectively.

Compared with **Figure 3**, it is obvious that the peak intensity of Ti(C, N, O) in **Figure 4** decreases with the removal of N_2 in the gas mixture, while that of TiO_2 increases, indicating that the amount of Ti(C, N, O) decreases in the product. It is worth noting that the Magnéli phase was not detected, which was not consistent with the thermodynamic calculation. It may be that the amount of Magnéli was too little to be detected by XRD, which has a relatively high detection limit about 1 ~ 2% of the sample [30, 31].

The quantitative results of Ti-bearing phases and the reduction degree have been listed in **Table 3**, and the conversion degree of Ti as a function with reduction temperature has been listed in **Table S3** and shown in **Figure 4(c)**, from the Rietveld refinement results. It is obvious that the conversion degree of Ti increases with the reduction temperature increasing in the range of 1000 ~ 1150 ºC. When above 1150 ºC, the conversion degree of Ti changes slowly. Compared with the CH_4-H_2-N_2 system, the conversion degree of Ti in the CH_4-H_2 system is much smaller. The addition of N_2 in the gas mixture can improve the carbonitriding process and lower the reaction temperature, as discussed above.

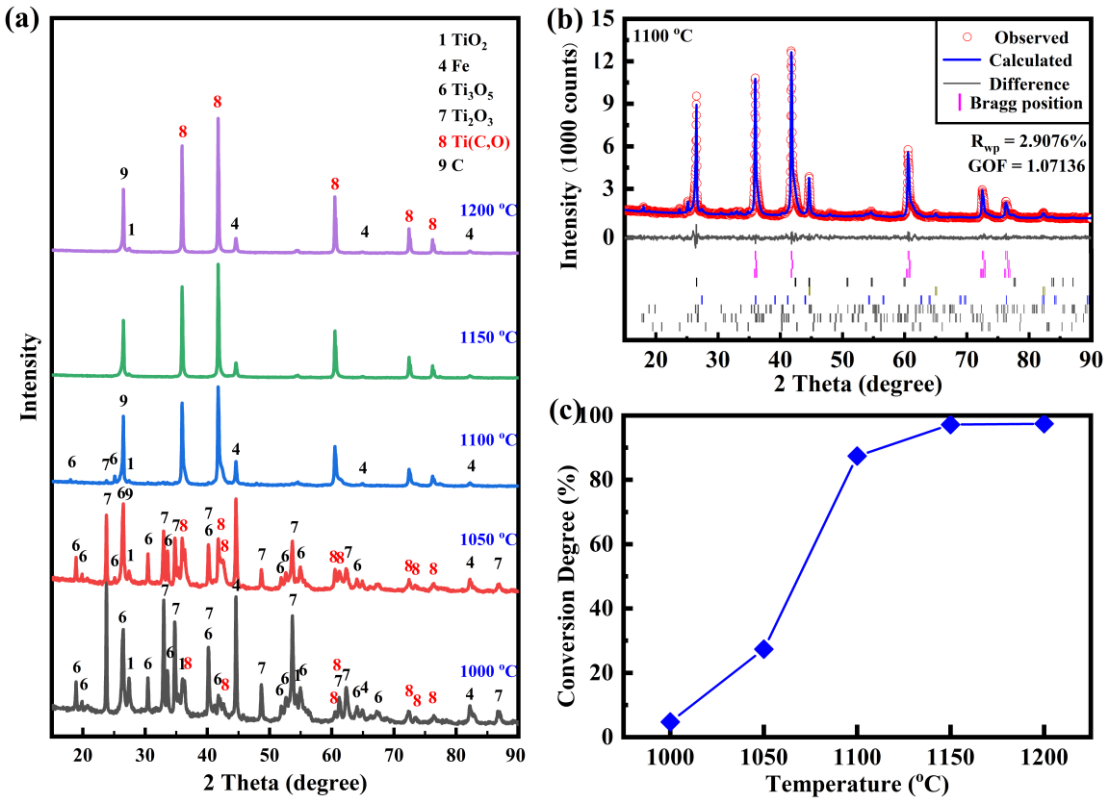

Figure 4 (a) XRD patterns of products reduced from TiO_2 with 10 wt.% Fe_2O_3 in 8 *vol*.% CH_4 – 92 *vol*.% H_2 gas mixture at 1100 °C for 1 hour; (b) Rietveld refinement of samples reduced at 1100 °C for 1 hour; (c) the function of Ti conversion degree with reduction temperature.

Table 3 Quantitative results of phases bearing titanium from the Rietveld refinement (corresponding to **Figure 4** and **Figure S5**) (*wt*.%)

Temperature (°C)	TiO_2	Ti_3O_5	Ti_2O_3	Ti(C, O)	Reduction degree (%)
1000	16.63	40.28	40.16	4.10	19.83
1050	6.49	32.91	36.62	24.10	34.34
1100	7.10	6.30	1.74	84.99	66.75
1150	3.58	-	-	96.42	73.36
1200	3.24	-	-	96.76	76.91

4.4 DFT study

For pure H_2 reduction, TiO_2 can only be reduced to Ti_3O_5 [32], while in addition CH_4, titanium oxides can be deeply reduced. To understanding the reduction mechanism and why N_2 can facilitate the reduction, the DFT calculation was carried out in this study. The adsorption of CH_4, H_2, and N_2 on the surface of TiO_2 is the prerequisite for the reduction occurring. Hence, the adsorption of gas molecules on the

surface of TiO_2 (110), which is the lowest energy surface and the active surface of TiO_2 [33], has been calculated, and the most stable structures have been shown in **Figure 5 (a) ~ (c)**, and the adsorption parameters are listed in **Table 4**. It can be observed that all of the gas molecules are adsorbed on the top of the Ti_{5c} atom of the TiO_2 (110) surface in the final stable structure. In the structure of CH_4 adsorption, the C atom of CH_4 sites above the Ti_{5c} atom of the surface. The most neighboring distances of H atom with Ti_{5c} atom and O atom are 2.606 and 2.602 Å, and those of C atom with Ti_{5c} atom and O atom are 3.030 and 3.454 Å, respectively. The corresponding adsorption energy (E_{ads}) is -0.365 eV, which is close to the result of Adam Kubas' study [34]. In the stable structure of H_2 adsorption, the H=H bond is parallel to the surface, and the most neighboring distance of H atom with Ti_{5c} atom and O atom are 2.438 and 2.748 Å, respectively. The adsorption energy of H_2 on the surface is -0.220 eV, which is higher than that of CH_4 on the surface. Combined with the thermodynamic analysis, it can be inferred that the difference between the reduction of TiO_2 with CH_4 and H_2 is caused by the thermodynamic and the adsorption: both the Gibbs free energies of CH_4 reacting with TiO_2 and the adsorption of CH_4 on the surface are lower than those of H_2. In the structure of N_2 adsorption, the N≡N bond is perpendicular to the TiO_2 (110) surface. The proximal N atom is located on the Ti_{5c} atom, agreeing to Xie's research [35], and the distance of the N-Ti atoms is 2.509 Å. The adsorption energy of N_2 on the surface is -0.376 eV, which is the most negative value among the three adsorption energies. It can explain that the addition of N_2 in the system can reduce the reaction temperature and improve the carbonitriding reaction.

Figure 5 (d) ~ (f) show the difference charge density maps for the adsorption structures of gas molecules on the surface of TiO_2 (110). The green region and yellow regions represent the electron-depleted region and the electron-accumulated region, respectively. From the difference charge density maps, it can be obtained that: (1) the yellow region between H_2 molecule and the surface of TiO_2 (110) is smaller than those of CH_4 molecule and N_2 molecule; (2) the green region of CH_4 adsorption model concentrates around the surrounding of H atoms and Ti_{5c} atom, and the yellow region concentrates between C atom and Ti_{5c} atom, indicating that some electrons translate from H and Ti_{5c} atoms to the region between C atom and Ti_{5c} atom; (3) the similar electrons translation can also be found in the adsorption of N_2 on the surface; (4) in the H_2 adsorption model, the electron translation of the TiO_2 (110) surface could not be found. These results indicate that the adsorption of H_2 is weaker than the other two,

which agrees well with the adsorption energy calculation results.

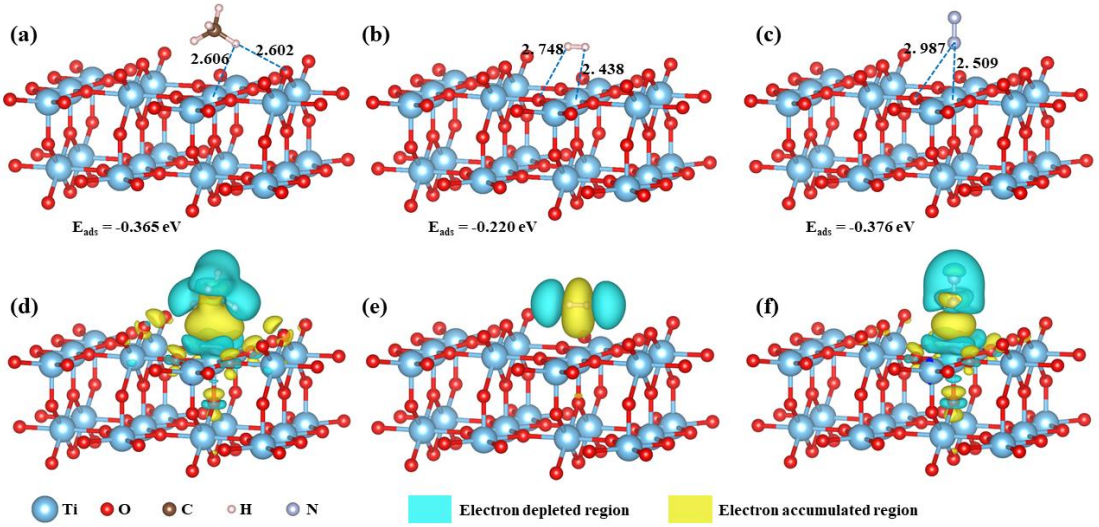

Figure 5 Adsorption structures of (a) CH_4, (b) H_2, (c) N_2 on the surface of TiO_2 (110); and difference charge density maps for the adsorption structures of (d) CH_4, (e) H_2, (f) N_2 on the surface.

Table 4 The adsorption energies (E_{ads}, eV) and adsorption configurations (d, Å) of gas molecules at their preferable adsorption sites

Species	E_{ads} (eV)	Adsorbate-surface atoms	d (Å)
CH_4	-0.365	H-Ti_{5c}	2.606
		C-Ti_{5c}	3.030
		H-O_{2c}	2.602
		C-O_{2c}	3.667
		H-O_{3c}	2.763
		C-O_{3c}	3.454
H_2	-0.220	H-Ti_{5c}	2.438
		H-O_{2c}	3.087
		H-O_{3c}	2.748
N_2	-0.376	N-Ti_{5c}	2.509
		N-O_{2c}	3.483
		N-O_{3c}	2.987

4.5 Reduction mechanism

Based on the above discussion, the reduction mechanism of TiO_2 in CH_4-H_2-N_2 gas mixture system was step-by-step reduction, as shown in **Figure 6**. It could be

divided into four stages: the reduction of ferric oxide, the formation of titanium suboxides, the formation of Ti(C, N, O) and the deep deoxygenation of Ti(C, N, O).

First, the Fe_2O_3 was reduced by CH_4 and H_2 to form the metallic iron (Fe), as following reactions:

$$Fe_2O_3 + 3H_2 = 2Fe + 3H_2O \quad (12)$$

$$Fe_2O_3 + 3CH_4 = 2Fe + 3CO + 6H_2 \quad (13)$$

The metallic iron (Fe) would play a role of catalyst in the following reductions, including methane pyrolysis [36], water-gas shift reaction [37], Boudouard reaction [38] and carbonitrided reaction of TiO_2.

Methane pyrolysis reaction: $CH_4 \overset{Fe}{\rightleftharpoons} C + 2H_2$ (14)

Water-gas shift reaction: $C + H_2O \overset{Fe}{\rightleftharpoons} CO + H_2$ (15)

Boudouard reaction: $C + CO_2 \overset{Fe}{\rightleftharpoons} 2CO$ (16)

Carbonitrided reaction of TiO_2:

$$TiO_2 + (2+x-z)CH_4 + 0.5yN_2 \overset{Fe}{=\!=} TiC_xN_yO_z + (2-z)CO + (4+2x-2z)H_2 \quad (17)$$

Second, the TiO_2 was reduced into titanium suboxides, including Magnéli phases, Ti_3O_5 and Ti_2O_3. Third, the titanium suboxides were carbonitrided into Ti(C, N, O). CH_4 would act as a carbonizing agent and N_2 would act as a nitridation agent in this stage. Last, the Ti(C, N, O) was deoxidized deeply.

In the whole process, H_2 had two important functions: reduction agent for reduction of Fe_2O_3 and TiO_2; balance gas for the CH_4 pyrolysis reaction to avoid the fast pyrolysis.

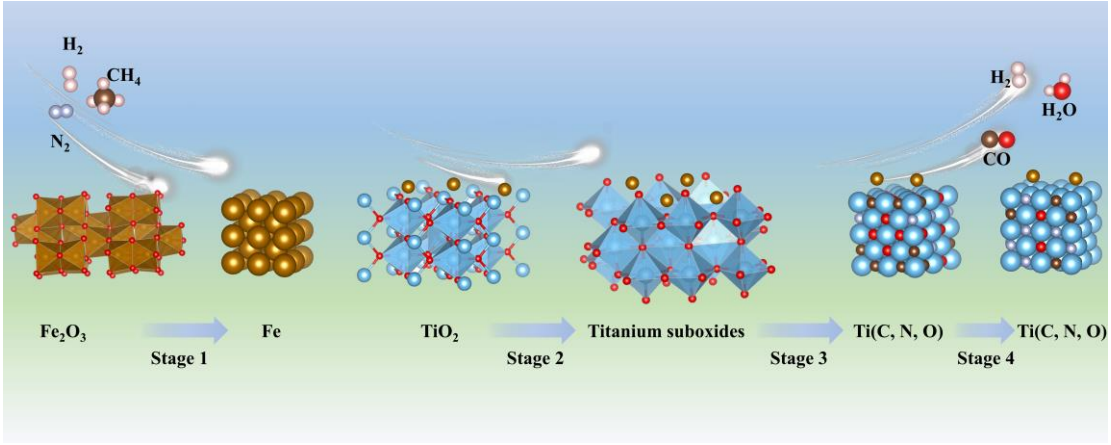

Figure 6 Schematic reaction mechanism of TiO_2 in CH_4-H_2-N_2 system

4.6 Process evaluation

In order to produce the titanium carbonitride, many methods have been proposed, some of which have been summarized in **Table 5**. Commercially, titanium carbide is usually synthesized from TiO_2 by carbothermic reduction process, at 1700 ~ 2100 ºC for 10 ~ 24 h. This method is the most mature technology and widely used. But the large energy consumption and long production cycle lead to the high production cost. The grades of TiO_2 and graphite have an important impact on the product quality. Other carbothermic methods also have the same disadvantages. The magnetron sputtering and plasma spray methods are usually used to coat a film on the surface of material, but cannot be used for mass preparation of Ti(C, N). Dewan used ilmenite and graphite to react at low temperature (1000 ~ 1300 ºC), but there exist a lot of titanium suboxides (Ti_2O_3, Ti_3O_5 …) in the product. Jiao and his colleagues could synthesize the pure $TiC_xN_yO_z$, but pure TiC, TiN and TiO as the raw material are required. Bai's method is similar to the hydrothermal method, but the temperature is higher than that of the hydrothermal method, and the pressure in the device is very high. Ammonia reduction method can reduce the reaction temperature, but NH_3 could corrode the equipment seriously and its cost is also very high. Zhang's group and our team have proposed the CH_4-bearing gas mixture reduction method, which proves that titanium-bearing mineral can reduced and carbonized at low temperature comparing with the commercial process. In this study, the CH_4-H_2-N_2 gas mixture has been used to reduce and carbonitride the TiO_2. It has been verified that the additive of N_2 can further lower the reduction temperature and promote the reaction rate. This method can also be applied in the reduction of ilmenite and titanium-bearing BF slag. Compared with the commercial method, the source of gas mixture is very extensive, such as nature gas, coke oven gas. The tail gas in this method is mainly composed of H_2, N_2, CO and a small amount of H_2O which can be removed. However, the product by this method is also a mixture phase, so it needs to be further refined to produce the high-quality product.

Table 5 Parameter comparison among some processes

Author	Raw materials	Atmosphere	Temperature	Time	Product	Reference
Commercial	TiO_2 + C	Ar / Vacuum	1700-2100 ºC	10~24h	Ti(C, O)	-
Shuqiang Jiao	TiO_2 + C	Vacuum	1400 ºC	4h	Ti_2CO	[39]
Kehan Wu	TiO_2 + C	N_2	1400-1600 ºC	8h	Ti(C, N)	[40]
M. A. R. Dewan	Ilmenite/rutile,	H_2, Ar, He	1000-1300 ºC	5h	Ti(C, O), C,	[41-43]

	graphite				Ti_2O_3, Ti_3O_5…	
Jiusan Xiao	TiC, TiN, TiO	Ar	1600 ºC	4h	$TiC_xN_yO_z$	[6]
Qiuyu Wang	TiC, TiN, TiO	-	1600 ºC	0.25h	$TiC_xN_yO_z$	[11]
Christian	TiC, TiN	Vacuum	500 ºC	4h	Ti(C, N)	[44]
Pengbo Mi	TiO_2, C	Ar, N_2	-	-	$TiC_{0.7}N_{0.3}$, Ti_3O	[45]
Yujun Bai	$TiCl_4$, CaC_2	N_2	500 ºC	8h	TiC + C	[12]
Yujun Bai	$TiCl_4$, $NaNH_2$	-	300 ºC	10 h	TiN	[13]
Miao Song	TiH_2	N_2, NH_3	1000 ºC	1.7h	TiN $TiN_{0.3}$	[46]
Yongjie Liu	TiO_2	NH_3	900-1200 ºC	3~8h	TiN_xO_{1-x}	[47]
Guangqing Zhang	TiO_2	CH_4, H_2, Ar	1300-1500 ºC	1.5-6h	TiC_xO_y, Ti_2O_3	[48]
Run Zhang	TiO_2, $CaTiO_3$	CH_4, H_2, Ar	1200-1450 ºC	8h	TiC_xO_y, Ti_3O_5	[24, 25]
Gangqiang Fan	Ilmenite, BF slag	CH_4, H_2, N_2	1150~1170 ºC	3-8h	Ti(C, N, O)	[22, 49]
This work	TiO_2	CH_4, H_2, N_2	1000-1200 ºC	0.5~1h	Ti(C, N, O)	-

5. Conclusion

This work describes the reduction and carbonitridation of TiO_2 with CH_4-H_2-N_2 gas mixture, through thermodynamic, experimental, and DFT studies. And some conclusions can be drawn as follows:

1. The reduction of TiO_2 is a step-by-step process: TiO_2 → Magnéli → Ti_3O_5 → Ti(N, C, O), and the gas composition and reaction temperature have significant impacts on the final products.
2. In the experimental product, the titanium carbonitride exists as a mixture of Ti(C, O), Ti(N, O), and Ti(C, N, O).
3. The reduction degree and the conversion degree of Ti increase with the reduction time, reduction temperature, and the addition of N_2 in the gas system.
4. The DFT study has indicated the adsorption energies of CH_4, H_2, and N_2 on the TiO_2 (110) surface are -0.365, -0.220, and -0.376 eV, respectively.
5. The method proposed in this work has shown a huge advantage and feasibility.

Acknowledgments

Thanks are given to the Fundamental Research Funds for National Natural Science Foundation of China (52074057), Graduate Scientific Research and Innovation Foundation of Chongqing (CYB19003), the Central Universities (2020CDJGFCL004), Fok Ying Tung Education Foundation (171111), the Venture & Innovation Support Program for Chongqing Overseas Returnees (cx2019041), Joint fund between Shenyang National Laboratory for Materials Science and State Key Laboratory of Advanced Processing and Recycling of Nonferrous Metals (18LHPY015), and Chongqing Postdoctoral Innovation Program (CQBX201904). Thanks are also given to the support from the school of chemistry and chemical engineering of Chongqing University for the DFT calculations.

Additionally, the authors also gratefully acknowledge the help of Mr. Qingyu Deng (Laboratory of Green Extractive Metallurgy for Polymetallic Mineral, Chongqing University), Ms. Yang Zhou and Ms. Hanjun Zou (Analytical and Testing Center, Chongqing University).

References

1. Baux, A.; Nouvian, L.; Arnaud, K.; Jacques, S.; Piquero, T.; Rochais, D.; David, P. and Chollon, G., *Synthesis and properties of multiscale porosity TiC-SiC ceramics.* Journal of the European Ceramic Society, 2019. **39**(8): 2601-2616.
2. R. Koc and Folmer, J. S., *Carbothermal synthesis of titanium carbide using ultrafine titania powders.* Journal of Materials Science, 1997. **32**(12): 3101-3111.
3. Rajabi, A.; Ghazali, M. J. and Daud, A. R., *Chemical composition, microstructure and sintering temperature modifications on mechanical properties of TiC-based cermet - A review.* Materials & Design, 2015. **67**: 95-106.
4. Rogachev, A. S.; Vadchenko, S. G.; Kochetov, N. A.; Kovalev, D. Y.; Kovalev, I. D.; Shchukin, A. S.; Gryadunov, A. N.; Baras, F. and Politano, O., *Combustion synthesis of TiC-based ceramic-metal composites with high entropy alloy binder.* Journal of the European Ceramic Society, 2020. **40**(7): 2527-2532.
5. Zhao, Shuaisheng; Gao, Xianghu; Qiu, Xiaoli; Yu, Dongmei and Tian, Guangke, *A novel TiC-TiN based spectrally selective absorbing coating: Structure, optical properties and thermal stability.* Infrared Physics & Technology, 2020. **110**: 103471.
6. Xiao, Jiusan; Jiang, Bo; Huang, Kai; Jiao, Shuqiang and Zhu, Hongmin, *Structural and Thermodynamic Properties of $TiC_xN_yO_z$ Solid Solution: Experimental Study and First-Principles Approaches.* Metallurgical and Materials Transactions A, 2016. **47**(9): 4721-4731.
7. Preiss, Henry; Bergerb, Lutz-Michael and Schultzec, Dietrich, *Studies on the Carbothermal Preparation of Titanium Carbide from Different Gel Precursors.* Journal of the European Ceramic Society, 1999. **19**: 195-206.
8. Ahmadi, E.; Suzuki, R. O.; Kikuchi, T.; Kaneko, T. and Yashima, Y., *Towards a sustainable technology for production of extra-pure Ti metal: Electrolysis of sulfurized Ti(C,N) in molten $CaCl_2$.* International Journal of Minerals Metallurgy and Materials, 2020. **27**(12): 1635-1643.

9. Takeda, Osamu; Ouchi, Takanari and Okabe, Toru H., *Recent Progress in Titanium Extraction and Recycling.* Metallurgical and Materials Transactions B, 2020. **51**(4): 1315-1328.
10. Wang, Qiuyu; Li, Yang; Jiao, Shuqiang and Zhu, Hongmin, *Producing metallic titanium through electro-refining of titanium nitride anode.* Electrochemistry Communications, 2013. **35**: 135-138.
11. Wang, Qiuyu; Song, Jianxun; Wu, Jinyu; Jiao, Shuqiang; Hou, Jungang and Zhu, Hongmin, *A new consumable anode material of titanium oxycarbonitride for the USTB titanium process.* Phys Chem Chem Phys, 2014. **16**(17): 8086-91.
12. Feng, Xin; Bai, Yujun; Lü, Bo; Wang, Chengguo; Liu, Yuxian; Geng, Guili and Li, Li, *Easy synthesis of TiC nanocrystallite.* Journal of Crystal Growth, 2004. **264**(1-3): 316-319.
13. Feng, Xin; Bai, Yujun; Lu, Bo; Wang, Chengguo; Qi, Yongxin; Liu, Yuxian; Geng, Guili and Li, Li, *Low temperature induced synthesis of TiN nanocrystals.* Inorganic chemistry, 2004. **43**(12): 3558-3560.
14. Xiang, Maoqiao; Song, Miao; Zhu, Qingshan; Hu, Chaoquan; Yang, Yafeng; Lv, Pengpeng; Zhao, Hongdan and Yun, Fen, *Facile synthesis of high‐melting point spherical TiC and TiN powders at low temperature.* Journal of the American Ceramic Society, 2019. **103**(2): 889-898.
15. Alexandrescu, R.; Borsella, E.; Botti, S.; Cesile, M. C. and Martelli, S., *Synthesis of TiC and SiC/TiC nanocrystalline powders by gas-phase laser-induced reaction.* Journal of Materials Science, 1997. **32**: 5629–5635.
16. Biedunkiewicz, Anna; Jasiński, Walenty; Lenart, Stanisz. Xl and Law, *Synthesis and growth of Ti-C coatings from the sol-gel process.* Vacuum, 1998. **50**(1): 65–68.
17. Sanada, Masafumi; Abe, Keisuke; Kurniawan, Ade; Nomura, Takahiro and Akiyama, Tomohiro, *Low-Temperature Synthesis of TiC from Carbon-Infiltrated, Nano-porous TiO_2.* Metallurgical and Materials Transactions B, 2020. **51**(5): 1958-1964.
18. Oyama, S. Ted and Schlatter, James C., *Preparation and characterization of early transition metal carbides and nitrides.* Industrial & Engineering Chemistry Research, 1988. **27**(9): 1639-1648.
19. Ostrovski, Oleg and Zhang, Guangqing, *Reduction and carburization of metal oxides by methane-containing gas.* AIChE Journal, 2006. **52**(1): 300-310.
20. Dang, Jie; Fatollahi-Fard, Farzin; Pistorius, Petrus Christiaan and Chou, Kuo-Chih, *Synthesis of Titanium Oxycarbide from Concentrates of Natural Ilmenite (Weathered and Unweathered) and Natural Rutile, Using a Methane-Hydrogen Gas Mixture.* Metallurgical and Materials Transactions B, 2017. **48**(5): 2440-2446.
21. Dang, Jie; Fatollahi-Fard, Farzin; Pistorius, Petrus Christiaan and Chou, Kuo Chih, *Synthesis of Titanium Oxycarbide from Titanium Slag by Methane-Containing Gas.* Metallurgical and Materials Transactions B, 2018. **49**(1): 123-131.
22. Fan, Gangqiang; Dang, Jie; Zhang, Run and Lv, Zepeng, *Synthesis of Ti(C, O, N) from ilmenite at low temperature by a novel reducing and carbonitriding approach.* International Journal of Energy Research, 2020. **44**(6): 4861-4874.
23. Fan, Gangqiang; Tan, Jundan; Zhang, Run; Dang, Jie; Bai, Chenguang; Lei, Huxu and Tan, Chaowen, *Crystallization and Carbonization of TiO_2–CaO–SiO_2 Ternary Slag*, in *Energy Technology 2020: Recycling, Carbon Dioxide Management, and Other Technologies*. 2020. 335-345.
24. Zhang, Run; Dang, Jie; Liu, Dong; Lv, Zepeng; Fan, Gangqiang and Hu, Liwen, *Reduction of*

perovskite-geikielite by methane–hydrogen gas mixture: Thermodynamic analysis and experimental results. Science of The Total Environment, 2019. **699**: 134355.

25. Zhang, Run; Liu, Dong; Fan, Gangqiang; Sun, Haibo and Dang, Jie, *Thermodynamic and Experimental Study on the Reduction and Carbonization of TiO_2 through Gas-Solid Reaction.* International Journal of Energy Research, 2019. **43**(9): 4253–4263.
26. Dudarev, S. L.; Botton, G. A.; Savrasov, S. Y.; Humphreys, C. J. and Sutton, A. P., *Electron-energy-loss spectra and the structural stability of nickel oxide: An LSDA+U study.* Physical Review B, 1998. **57**(3): 1505-1509.
27. Morgan, Benjamin J. and Watson, Graeme W., *A DFT+U description of oxygen vacancies at the TiO_2 rutile (110) surface.* Surface Science, 2007. **601**(21): 5034-5041.
28. Becke, Axel D. and Johnson, Erin R., *Exchange-hole dipole moment and the dispersion interaction.* The Journal of Chemical Physics, 2005. **122**(15): 154104.
29. Cao, Zhanmin; Xie, Wei; Jung, In-Ho; Du, Guangwei and Qiao, Zhiyu, *Critical Evaluation and Thermodynamic Optimization of the Ti-C-O System and Its Applications to Carbothermic TiO_2 Reduction Process.* Metallurgical and Materials Transactions B, 2015. **46**(4): 1782-1801.
30. Dutrow, Barbara L. and Clark, Christine M. *X-ray Powder Diffraction (XRD)*. Available from: https://serc.carleton.edu/research_education/geochemsheets/techniques/XRD.html.
31. Schwartz, D., *ITWG Guideline on Powder X-ray Diffraction (XRD) - General Overview*. 2015, Nuvlear Forensics International Technical Working Group.
32. Dang, Jie; Zhang, Guo-Hua and Chou, Kuo-Chih, *Kinetics and mechanism of hydrogen reduction of ilmenite powders.* Journal of Alloys and Compounds, 2015. **619**: 443-451.
33. Comer, Benjamin M. and Medford, Andrew J., *Analysis of Photocatalytic Nitrogen Fixation on Rutile TiO_2 (110).* ACS Sustainable Chemistry & Engineering, 2018. **6**(4): 4648-4660.
34. Kubas, Adam; Berger, Daniel; Oberhofer, Harald; Maganas, Dimitrios; Reuter, Karsten and Neese, Frank, *Surface Adsorption Energetics Studied with "Gold Standard" Wave-Function-Based Ab Initio Methods: Small-Molecule Binding to TiO_2 (110).* J Phys Chem Lett, 2016. **7**(20): 4207-4212.
35. Xie, Xiaoying; Xiao, Pin; Fang, Weihai; Cui, Ganglong and Thiel, Walter, *Probing Photocatalytic Nitrogen Reduction to Ammonia with Water on the Rutile TiO_2 (110) Surface by First-Principles Calculations.* Acs Catalysis, 2019. **9**(10): 9178-9187.
36. Ermakova, M. A.; Ermakov, D. Y.; Chuvilin, A. L. and Kuvshinov, G. G., *Decomposition of methane over iron catalysts at the range of moderate temperatures: The influence of structure of the catalytic systems and the reaction conditions on the yield of carbon and morphology of carbon filaments.* Journal of Catalysis, 2001. **201**(2): 183-197.
37. Aragao, I. B.; Ro, I.; Liu, Y. F.; Ball, M.; Huber, G. W.; Zanchet, D. and Dumesic, J. A., *Catalysts synthesized by selective deposition of Fe onto Pt for the water-gas shift reaction.* Applied Catalysis B-Environmental, 2018. **222**: 182-190.
38. Bost, N.; Ammar, M. R.; Bouchetou, M. L. and Poirier, J., *The catalytic effect of iron oxides on the formation of nano-carbon by the Boudouard reaction in refractories.* Journal of the European Ceramic Society, 2016. **36**(8): 2133-2142.
39. Jiao, Shuqiang and Zhu, Hongmin, *Novel Metallurgical Process for Titanium Production.* Journal of Materials Research, 2006. **21**(9): 2172-2175.
40. Wu, Ke-Han; Jiang, Yu; Jiao, Shu-Qiang; Chou, Kuo-Chih and Zhang, Guo-Hua, *Preparations of titanium nitride, titanium carbonitride and titanium carbide via a two-step carbothermic*

reduction method. Journal of Solid State Chemistry, 2019. **277**: 793-803.

41. Dewan, Mohammad A. R.; Zhang, Guangqing and Ostrovski, Oleg, *Carbothermal Reduction of Titania in Different Gas Atmospheres.* Metallurgical and Materials Transactions B, 2008. **40**(1): 62-69.
42. Dewan, Mohammad A. R.; Zhang, Guangqing and Ostrovski, Oleg, *Carbothermal Reduction of a Primary Ilmenite Concentrate in Different Gas Atmospheres.* Metallurgical and Materials Transactions B, 2009. **41**(1): 182-192.
43. Dewan, M. A. R.; Zhang, G. Q. and Ostrovski, O., *Carbothermal reduction of ilmenite concentrates and synthetic rutile in different gas atmospheres.* Mineral Processing and Extractive Metallurgy, 2013. **120**(2): 111-117.
44. Saringer, Christian; Kickinger, Christoph; Munnik, Frans; Mitterer, Christian; Schalk, Nina and Tkadletz, Michael, *Thermal expansion of magnetron sputtered TiCxN1-x coatings studied by high-temperature X-ray diffraction.* Thin Solid Films, 2019. **688**.
45. Mi, Pengbo; He, Jining; Qin, Yanfang and Chen, Kai, *Nanostructure reactive plasma sprayed TiCN coating.* Surface and Coatings Technology, 2017. **309**: 1-5.
46. Song, M.; Xiang, M. Q.; Yang, Y. F.; Zhu, Q. S.; Hu, C. Q. and Lv, P. P., *Synthesis of stoichiometric TiN from TiH2 powder and its nitridation mechanism.* Ceramics International, 2018. **44**(14): 16947-16952.
47. Liu, Yongjie; Wang, Yue; Zhang, Yu; You, Zhixiong and Lv, Xuewei, *Mechanism on reduction and nitridation of micrometer‐sized titania with ammonia gas.* Journal of the American Ceramic Society, 2020. **103**(6): 3905-3916.
48. Zhang, Guangqing and Ostrovski, Oleg, *Reduction of titania by methane-hydrogen-argon gas mixture.* Metallurgical and Materials Transactions B, 2000. **31B**: 129-139.
49. Fan, Gangqiang; Wang, Meng; Dang, Jie; Zhang, Run; Lv, Zepeng; He, Wenchao and Lv, Xuewei, *A novel recycling approach for efficient extraction of titanium from high-titanium-bearing blast furnace slag.* Waste Management, 2021. **120**: 626-634.

Figures

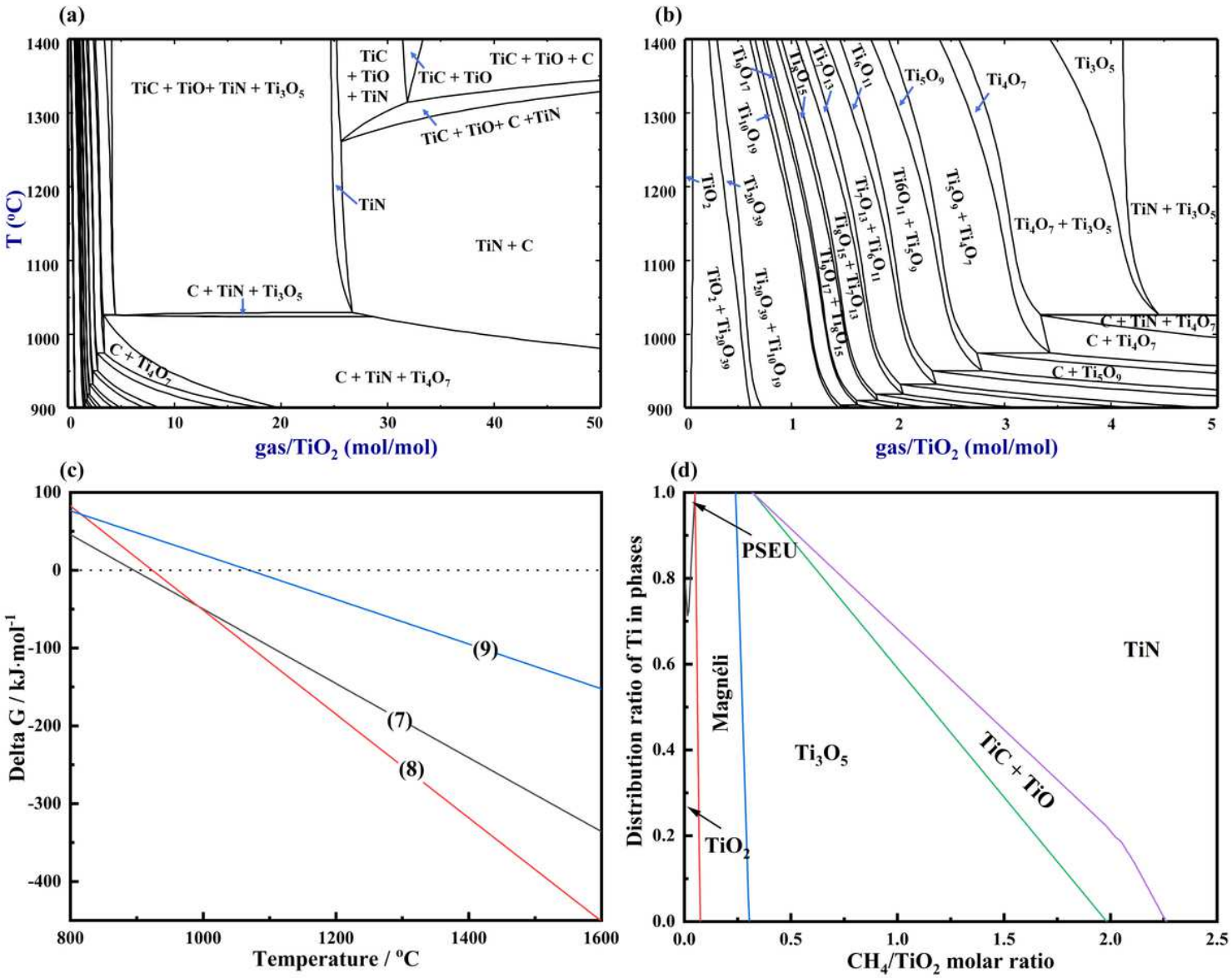

Figure 1

(a) Calculated equilibrium phase diagram of solid phases as functions of temperature and the gas/TiO2 ratio (gas = 8 vol.% CH4 – 16 vol.% N2 – 76 vol.% H2) and (b) partial diagram of (a); (c) the Gibbs free energy of equation (7)~ (9) as a function of temperature; (d) calculated equilibrium of titanium-bearing phases for the reaction of TiO2 with Fe2O3 additive in 8 vol.% CH4-8 vol.% N2-84 vol.% H2 gas mixture at 1200 oC.

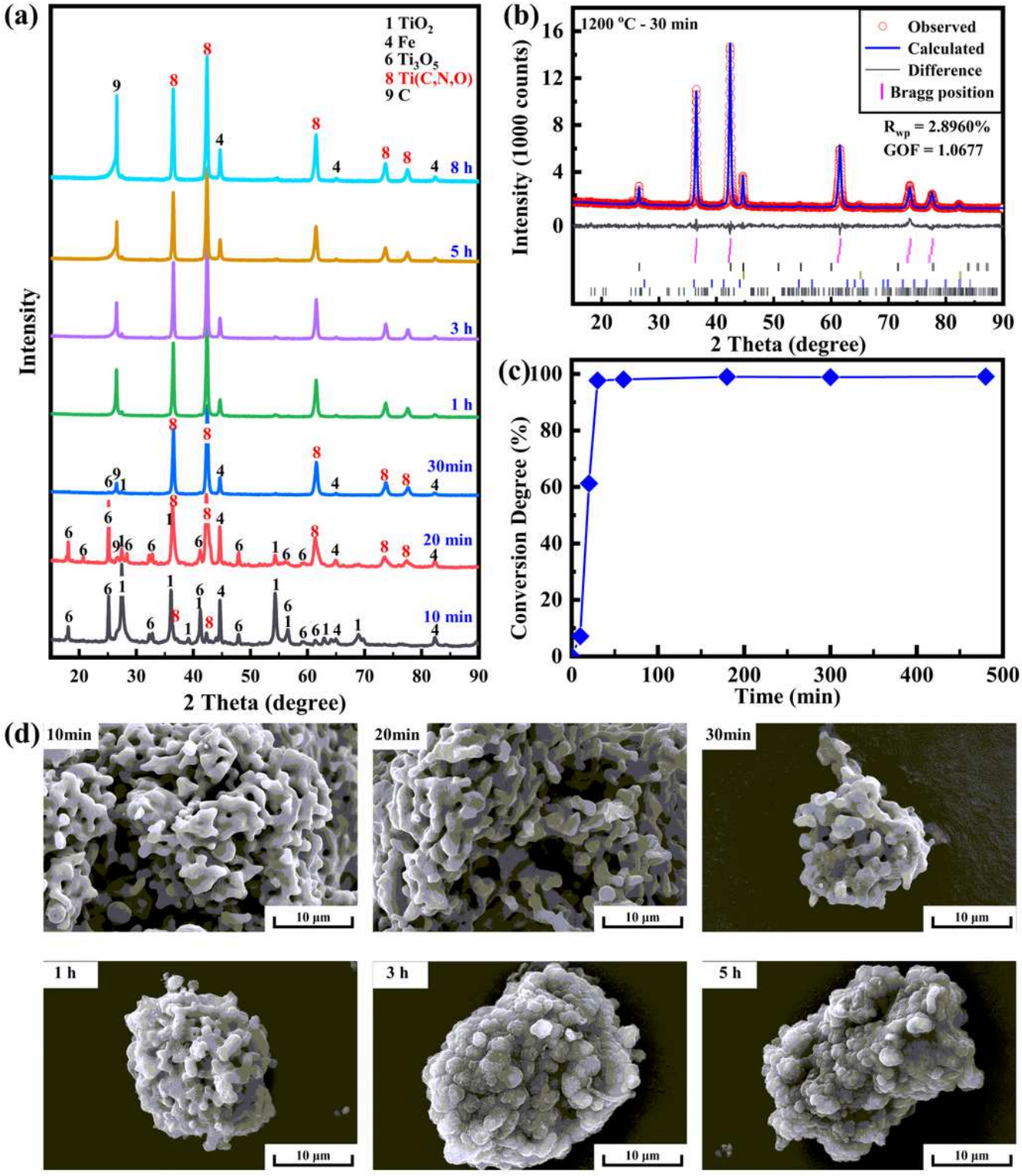

Figure 2

(a) XRD patterns of reduced samples for different reaction times at 1200 oC in 8 vol.% CH4 - 16 vol.% N2 - 76 vol.% H2; (b) Rietveld refinement results from the XRD patterns; (c) the function of Ti conversion degree with reduction time; (d) SEM images of samples reduced for different times.

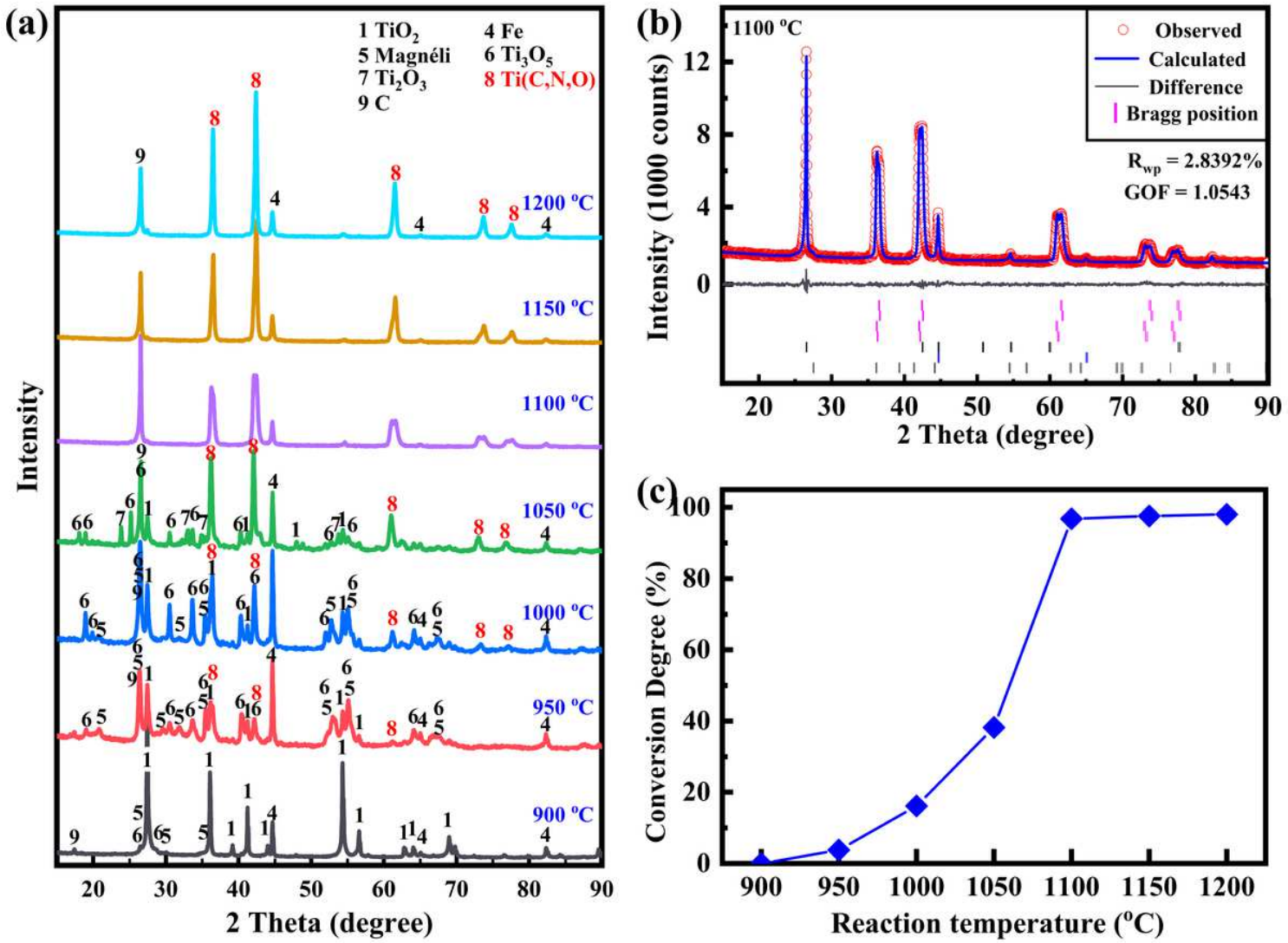

Figure 3

(a) XRD patterns of samples reduced at different temperatures for 1 h in 8 vol.% CH4 - 16 vol.% N2 - 76 vol.% H2; (b) Rietveld refinement results from the XRD patterns; (c) the function of Ti conversion degree with the reaction temperature.

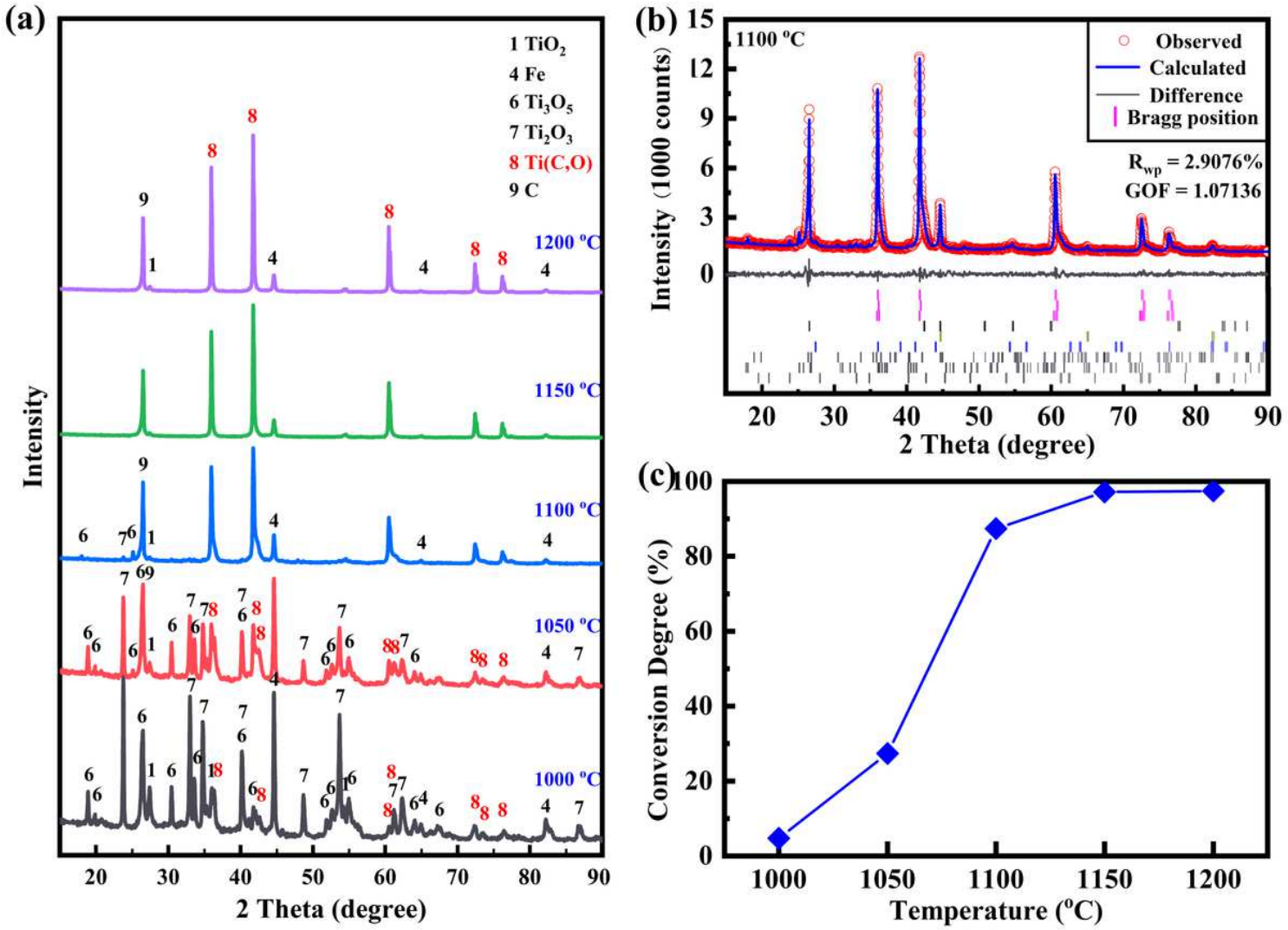

Figure 4

(a) XRD patterns of products reduced from TiO2 with 10 wt.% Fe2O3 in 8 vol.% CH4 – 92 vol.% H2 gas mixture at 1100 oC for 1 hour; (b) Rietveld refinement of samples reduced at 1100 oC for 1 hour; (c) the function of Ti conversion degree with reduction temperature.

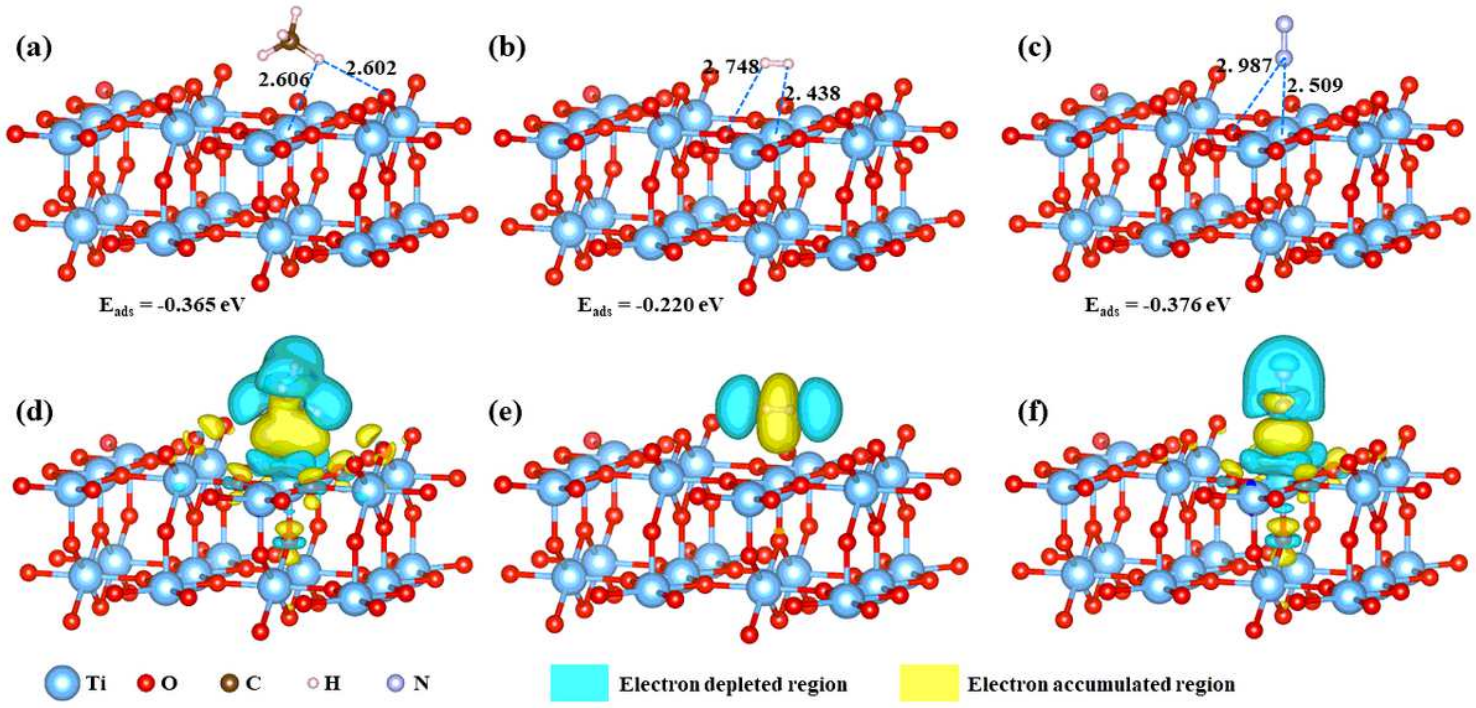

Figure 5

Adsorption structures of (a) CH4, (b) H2, (c) N2 on the surface of TiO2 (110); and difference charge density maps for the adsorption structures of (d) CH4, (e) H2, (f) N2 on the surface.

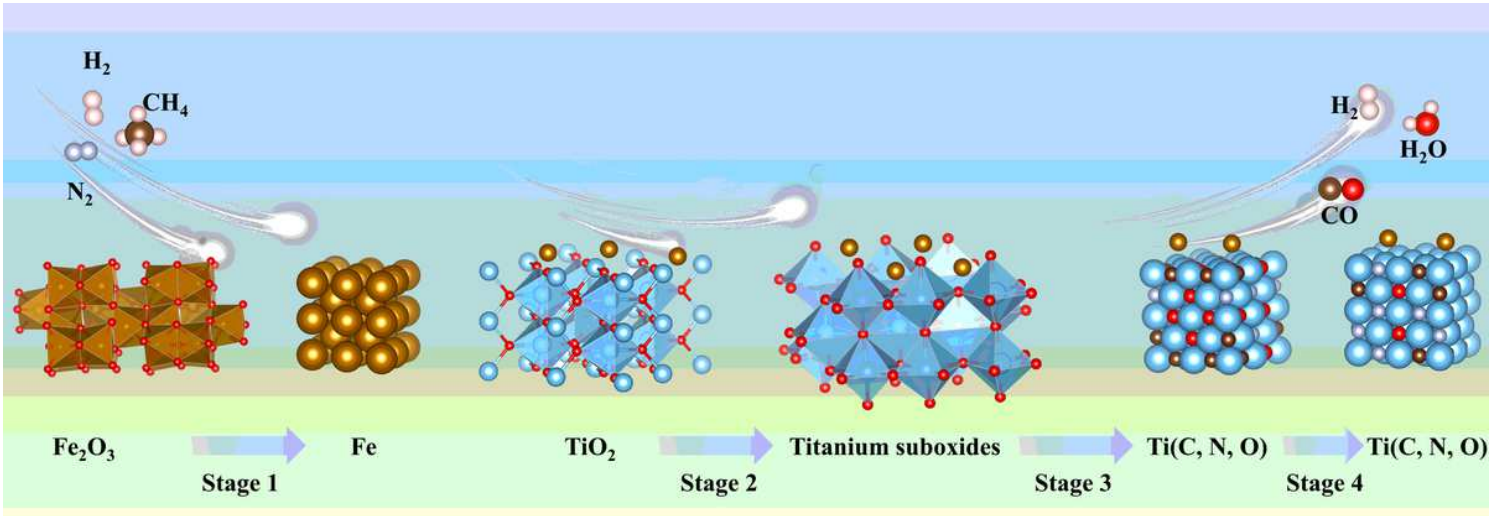

Figure 6

Schematic reaction mechanism of TiO2 in CH4-H2-N2 system

Supplementary Files

This is a list of supplementary files associated with this preprint. Click to download.

- ElectronicSupplementaryInformation.docx